Corrosion of nickel-based structural materials for nuclear reactors by molten fluoride salt: From bulk content of corrosion products to elemental imaging of corrosion changes

T. Warchilová, V. Dillingerová, R. Škoda, T. Šimo, O. Matal, T. Vaculovič, V. Kanický

PII: S0584-8547(17)30582-7
DOI: doi:10.1016/j.sab.2018.06.010
Reference: SAB 5467

To appear in: *Spectrochimica Acta Part B: Atomic Spectroscopy*

Received date: 27 November 2017
Revised date: 12 June 2018
Accepted date: 13 June 2018

Please cite this article as: T. Warchilová, V. Dillingerová, R. Škoda, T. Šimo, O. Matal, T. Vaculovič, V. Kanický , Corrosion of nickel-based structural materials for nuclear reactors by molten fluoride salt: From bulk content of corrosion products to elemental imaging of corrosion changes. Sab (2018), doi:10.1016/j.sab.2018.06.010

Corrosion of nickel-based structural materials for nuclear reactors by molten fluoride salt: From bulk content of corrosion products to elemental imaging of corrosion changes

T. Warchilová,[ab] V. Dillingerová [ab], R. Škoda,[c] T. Šimo,[d] O. Matal,[d], T. Vaculovič,[ab*] V. Kanický[ab]

[a]Laboratory of Atomic Spectrochemistry, Department of Chemistry, Faculty of Science, Masaryk University, Kotlářská 2, 611 37 Brno, Czech Republic
[b]Central European Institute of Technology, Masaryk University, Kamenice 5, 625 00 Brno, Czech Republic
[c]Department of Geological Sciences, Faculty of Science, Masaryk University, Kotlářská 2, 611 37 Brno, Czech Republic
[d]ENERGOVÝZKUM, spol. r. o., Božetěchova 17, 612 00 Brno, Czech Republic

E-mail: vaca@mail.muni.cz

Abstract

This work is focused on the study of corrosion treatment of molten fluoride salt (MFS) on three candidate structural materials (Ni, ferritic steel with protective Ni coating, and Ni-based alloy). The samples were exposed to an MFS mixture (60 mol% LiF + 40 mol% NaF) at a temperature of 680 °C for 112, 350 and 1000 hours. Their corrosion resistance was tested by the determination of the content of corrosion products in MFS by ICP-OES (Inductively Coupled Plasma with Optical Emission Spectrometry) analysis and comparison of elemental ratios. Distinctive differences in the ratios were found for ferritic steel with protective Ni coating. Morphological changes induced by MFS treatment were revealed and studied by EPMA (Electron Probe Micro Analysis) and LA-ICP-MS (Laser Ablation Inductively Coupled Plasma of Mass Spectrometry). Elemental maps of the corroded area were acquired by both methods. The analyses of corrosion products show that the best candidate material is nickel.

Key words: molten fluoride salt, LA-ICP-MS, EPMA, corrosion, elemental imaging, Ni-based structural material

1. Introduction

The Molten Salt Reactor (MSR) is a promising nuclear reactor type, which belongs to the group of Generation IV reactor systems [1]. The great benefits of this reactor design are its efficient fuel utilization, minimum radioactive waste and economical use with a safe and environmentally friendly operation [2-4]. Molten salts, exhibit the most appealing properties; they can be used as reactor coolant or a transfer medium in high temperature process heat loops from nuclear reactors to hydrogen production. This explains why they were taken into consideration in the development of nuclear energy technology.

These salts are characterized by a high thermal conductivity, low viscosity, high boiling points, the largest heat capacity per unit volume without any need of pressurization, and insensitivity to radiation [4]. Compared to chloride salts, fluoride salts are more frequently used because fluorine does not require an expensive isotope separation process. Potential

coolants for MSR's are BeF_2-salts and alkali fluoride salts. The construction of MSR is a complex process with many difficulties such as finding compatible and resistant structural material for the application and development of the system. The chemical attack of MFS at working temperature level (570 °C) is highly corrosive. The corrosion in MFS is driven by several factors involving thermodynamic aspects such as Gibbs free energy of fluorides formation, corrosion due to the presence of impurities (moisture, oxygen, metals) and fission products [5]. Alloy dissolved from hotter zones is transported by convection and then plated to colder areas. The major impurities must be removed in order to prevent severe corrosion of the container metal. Typical impurities include moisture and oxide contaminants, which together with a temperature gradient and galvanic corrosion are considered the main driving forces for the corrosion [6, 7]. Additionally, alloying elements dissolved into molten salts accelerate the corrosion due to thermodynamic transportation [8, 9]. Moreover, the production of helium due to neutron irradiation and the formation of helium bubbles can cause extreme swelling, surface roughening and surface blistering [10].

The most promising corrosion-resistant structural materials are Ni-based alloys, e.g. Monels, Inconels, Hastelloys, pure nickel and Ni-plated alloys [11-13]. The tendency for common alloying constituents to corrode in MFS increases in the order of Ni, Co, Fe, Cr and Al, with Al being the most prone to dissolution [14].

Electrochemical techniques such as voltammetry are ideal for the study of corrosion thermochemistry and kinetics [15, 16]. For the investigation of the corrosion processes of materials various measurement techniques are typically applied, including e.g. Scanning Electron Microscopy (SEM) [13, 17], EPMA [17], synchrotron radiation techniques [13], laser ablation based methods - LA-ICP-MS [18, 19] and Laser Induced Breakdown Spectroscopy (LIBS) [20, 21].

This work is devoted to the study of the corrosion behavior of three candidate structural materials when exposed to MFS treatment for variuos time. Resistance to corrosion of ferritic steel with protective Ni coating, Ni, and Ni-based alloy A071EV was expressed and compared in terms of content of steel constituents dissolved in MFS and their elemental ratios. The dissolution of particular steel constituents in MFS was assessed based on the determination of corrosion products in exposed MFS by ICP-OES solution analysis. Elemental maps of corroded area over the Ni-coating/steel substrate interface on a perpendicular section were acquired by EPMA and LA-ICP-MS.

2. Experimental

2.1. Corrosion test

The ferritic steel S355 J0 (>95 $\%_{w/w}$ Fe) coated with an 80 μm nickel protective layer, nickel (99.0 $\%_{w/w}$ Ni, 0.80 $\%_{w/w}$ Fe, 0.20 $\%_{w/w}$ Mn), and A071EV alloy (in $\%_{w/w}$: 76.3 Ni, 7.0 Cr, 4.5 W, 9.0 Mo and 1.7 Ti) were tested as candidate structural materials. For this purpose, the specimen (rectangular prism, 2×5×7 mm) of investigated material was suspended into an ampoule (height 185 mm, inner diameter 21.3 mm, wall thickness 2 mm) made of the same material. The ampoule was filled with the mixture of LiF-NaF (60:40 by mol%) of certified elemental composition 12.9 $\%_{w/w}$ Li, 28.4 $\%_{w/w}$ Na, and 58.7 $\%_{w/w}$ F. The ampoule was evacuated and then heated to 200 °C for 2 hours for degassing, after which it was maintained

at a constant test temperature of 680 °C in a furnace with an argon atmosphere thus preventing oxygen penetration. After the isothermal exposure (112, 350 and 1000 hours) the ampoule and the specimen were allowed to cool to room temperature.

2.2. Determination of corrosion products in MFS and preparation of the test specimen for elemental mapping

The ampoule with the specimen was cut along its axis, the test sample was removed and the solidified fluoride mixture was separated and ground in a ball mill. A 250 mg portion of homogenized fluoride mixture was dissolved in nitric acid, diluted to 250 ml and the resulting solution was used to determine the corrosion products (Ni, Fe, Mn, Cr, W, Mo, and Ti) by the ICP-OES Jobin-Yvon 170 Ultrace (Jobin-Yvon, France) [22, 23]. The Ni-coated steel specimen was cut with a diamond saw and both resulting parts were embedded into epoxy resin disks (Araldite®, Huntsman Advanced Materials), lapped and polished with diamond paste for EPMA and LA-ICP-MS elemental mapping.

2.3. EPMA/WDS and LA-ICP-MS elemental mapping of corroded Ni-steel interface

The spatial 2D distribution of elements of interest was determined by means of electron probe microanalyser Cameca SX100. The X-Ray maps were collected at an accelerating voltage of 15 kV, beam current of 40 nA, beam diameter < 1 µm. The *K*α X-rays of F, Na, Cr, Fe, and Ni were simultaneously collected in the wavelength-dispersion mode (WDS) on PC1, TAP, PET, PET and LIF monochromators, respectively. The grid of the map was set at 250 x 188 pixels with a step size of 3 µm to cover an area of 747 x 561 μm^2. The dwell (counting) times for the peak and the background were 250 ms each. The stage-moving mode at static beam was chosen to keep the detector, monochromator and X-ray source aligned in ideal geometry. The background intensities were subtracted from the peak intensities for further data interpretation. The acquired data were quantified using albite (Na), CaF_2 (F), and pure metals Cr, Fe, Ni as calibrants and X-PHI matrix correction routine [24].

The UP213 laser ablation system with a 213 nm lasing wavelength and a 4.2 ns pulse width (New Wave Research, Inc., ESI, Fremont, CA, USA) coupled with the quadrupole ICP-MS Agilent 7500ce (Agilent Technologies, Japan) was used for elemental mapping. The operating parameters of the LA-ICP-MS experiments were the same as used in previous work [19]. The analysed area was the same as for EPMA elemental mapping. For the ablation series of individual non-overlapped spots were used. The distance between spots in one line and between lines was 8 µm. Each row of isolated ablation spots originated outside the test specimen in the epoxy resin material, continued through the Ni-coating and coating/substrate interface into the corroded area of steel substrate and ended in the unaffected substrate zone. The quantification was performed using the total sum of signals of isotopes [19, 23].

3. Results and discussion

3.1. Determination of corrosion products in exposed MFS and evaluation of corrosion resistance

The content of corrosion products in MFS is an indicator for the selection of the most resistant material. The results of ICP-OES solution analysis of MFS are summarized in Table 1. Generally, corrosion rate decreases with exposure time for all constituents, but it differs for particular elements. Due to the substantially lower content of Cr, W, Mo and Ti in nickel coating and in nickel the amount of these elements released by corrosion into MFS is lower than the LOD of the ICP-OES method. The relative standard deviation (RSD) of the analysis ranges from 1 to 7 % except for values of content near to the LOD where the RSD increased to 20 %.

The comparison of total content values of corrosion products in MFS for each period of exposure indicates that both the coated steel and Ni is more resistant than A071EV alloy. The total content values of corrosion products released from coated steel and Ni into MFS after 112 and 350 hours of exposure are very close, whereas 1000 h exposure results in a significantly higher amount of corrosion products coming from coated steel than from Ni. The content of elements in MFS differs distinctly depending on examined candidate material. The ratios of Fe/Ni, Mn/Ni, (and where possible also of Cr/Ni, W/Ni, Mo/Ni and Ti/Ni) were calculated both for original (intact) structural materials and for MFS after exposure in order to compare the individual candidate materials in terms of corrosion rate. The content of corrosion products in MFS is nonlinear increasing with time. The steep increase of corrosion products during the first 112 h is observed for all candidate material, can be caused by the presence of impurities in the system, mainly moisture in the MFS that reacts with fluorides to form highly corrosive HF [5]. This observation is consistent with Koger who found that the amount of Cr in MFS after the first 3 hours of exposure was 25 mg/kg and increased to 551 mg/kg after 30000 hours [25]. Moreover, the corrosion rate is driven by diffusion of the metals from the alloy surface into the MFS [26]. The diffusion slows down due to equalization of the concentration on the alloy-MFS interface. They observed that the long-term corrosion attack can be predicted by a logarithmic fitting curve.

	Corrosion products content in MFS ($\%_{w/w}$)							
Exposure time (h)	Ni	Fe	Mn	Cr	W	Mo	Ti	Total content
				Ni-coated S355 J0 steel				
112	0.0019	0.0198	0.0014	<	<	<	<	0.0231
350	0.0044	0.0215	0.0029	<	<	<	<	0.0287
1000	0.0067	0.0464	0.0069	<	<	<	<	0.0599
				Ni				
112	0.0164	0.0039	0.0008	<	<	<	<	0.0211
350	0.0195	0.0055	0.0017	<	<	<	<	0.0267
1000	0.0320	0.0072	0.0031	<	<	<	<	0.0423
				Alloy A071EV				
112	0.0056	0.0012	0.0008	0.0011	0.0190	0.0270	0.0036	0.0584
350	0.0083	0.0036	0.0012	0.0012	0.0229	0.0193	0.0047	0.0612
1000	0.0150	0.0067	0.0035	0.0010	0.0224	0.0219	0.0054	0.0758
				LOD ($\%_{w/w}$)				
	0.0002	0.0005	0.00005	0.0001	0.001	0.001	0.0005	

Table 1: Content of corrosion products in MFS resulting from exposure of nickel-coated steel S355 J0, nickel, and alloy A071EV depending on the time of exposure.

	Exposure (h)	Fe/Ni	Mn/Ni	Cr/Ni	W/Ni	Mo/Ni	Ti/Ni
Ni-coated S355 J0	112	10.7	0.76	-	-	-	-
	350	4.9	0.65	-	-	-	-
	1000	7.0	1.0	-	-	-	-
	intact	0.002	0.008	-	-	-	-
Ni	112	0.24	0.051	-	-	-	-
	350	0.28	0.087	-	-	-	-
	1000	0.22	0.095	-	-	-	-
	intact	0.002	0.008	-	-	-	-
alloy A071EV	112	0.21	0.15	0.20	3.3	4.8	0.64
	350	0.43	0.15	0.14	2.8	2.3	0.56
	1000	0.45	0.23	0.16	1.5	1.5	0.36
	intact	0.001	0.001	0.092	0.059	0.118	0.022

Table 2: Ratio of content of corrosion products to content of Ni in MFS resulting from exposure of nickel-coated steel S355 J0, nickel, and alloy A071EV depending on the time of exposure and their ratio of intact material

		$w_{LiFNaF}/w_{material}*10^3$						
	Exposure (h)	Ni	Fe	Mn	Cr	W	Mo	Ti
Ni-coated S355 J0	112 h	0.019	99	1.8	-	-	-	-
	350 h	0.044	107	3.6	-	-	-	-
	1000 h	0.067	232	8.6	-	-	-	-
Ni	112 h	0.165	19	1.0	-	-	-	-
	350 h	0.197	27	2.1	-	-	-	-
	1000 h	0.323	36	3.8	-	-	-	-
alloy A071EV	112 h	0.074	12	12	0.16	4.2	3.0	2.1
	350 h	0.109	36	17	0.17	5.1	2.1	2.8
	1000 h	0.197	67	50	0.14	5.0	2.4	3.2

Table 3: Ratio of content of particular element in MFS after exposure to its content in intact material

It is evident from Table 2 that pronounced enrichment of Fe and Mn (and also of Cr, W, Mo and Ti where determinable) occurred with respect to Ni in exposed salt in comparison to elemental ratios in all three intact materials. The most conspicuous enrichment of Fe and Mn in MFS is observed for Ni-coated steel (10.7 *vs.* 0.002 in MFS and intact material, respectively). It is remarkable that this enrichment is substantially higher for Ni-coated steel than for Ni, although the coating material and "bulky" Ni have the same composition (99 $\%_{w/w}$ Ni, 0.8 $\%_{w/w}$ Fe, 0.2 $\%_{w/w}$ Mn). Thus, it can be assumed that corrosion occurred mainly on the coating/substrate interface and the increased content of Fe (Mn) might predominantly originate from steel substrate. Corrosion products than probably penetrate into

the MFS through the damaged nickel coating. To confirm this assumption, a section of the exposed specimen of Ni-coated steel was subjected to surface imaging by EPMA. It is obvious from the EMPA image of the section (Fig. 2) that porous caverns developed in the steel substrate in positions opposite the areas of distinctly thinned nickel coating. Due to different thermal expansion coefficients of Ni and Fe (13 and 12 μm/K) the micro cracks probably existed at locations of thinned Ni-coating before MFS attack or they formed during the test due to increased temperature, and MFS consequently came into contact with the steel substrate. Thus provoked corrosion has produced an increased content of substrate constituents in MFS. Diffusion and convection during the test transported corrosion products outside the specimen into MFS.

The significant rise of the Fe/Ni ratio in MFS with increasing exposure time is observed for the nickel-based alloy A071EV (Table 2) which indicates that the rate of Fe release from the alloy into MFS was higher than that of Ni. Different corrosion rates for Ni and Fe are also evident from Table 1. On the other hand, the Mn/Ni and Cr/Ni ratios in MFS remain approximately the same during exposure. Besides, the Mn/Ni ratio is increased in MFS in comparison to the intact specimen by two orders while Cr/Ni ratio no more than twice. Different behavior is visible for W/Ni, Mo/Ni, and Ti/Ni. Important enrichment of W, Mo, and Ti in fluoride salt occurred during 112 h, however, W/Ni, Mo/Ni and Ti/Ni ratios then decrease with increasing MSR exposure. The decrease in these ratios is related to the fact that the amount of Ti, Mo and W increases in the MFS more slowly than the amount of Ni. This may be due to the fact that the amount of Ti, Mo and W in the MFS is close to their amount on the surface of the alloy and their diffusion slows down.

The resistance of the candidate material to the LiF-NaF exposure can be scored as a ratio of the content of given elements in the LiF-NaF mixture after exposure (w_{LiFNaF}) to the content of particular elements in the tested material ($w_{material}$), as well. The most resistant elements exhibit the lowest ratio and *vice versa*. It is evident from Table 3 that nickel is the most resistant element to MFS exposure whereas iron is the most susceptible to corrosion. The noticeable enrichment in the case of Ni-coated steel is caused by preferential corrosion of steel substrate that occurred by penetration of nickel coating by MFS to iron substrate as is clearly seen in Fig. 1. In case of alloy A071EV the most resistant elements are Ni and Cr. Ni, Fe, Mn exhibit similar behavior – a significant enrichment in LiF-NaF mixture with increasing time of exposure (Tab 1 and Tab 3). On the contrary, in the case of Cr, W, and Mo no significant enrichment is observed. For Ti, slight enrichment occurred. The behavior of Cr, W, Mo and Ti could be caused by their passivation which suppresses the corrosion rate. The results from Tables 2 and 3 show the same conclusion regarding the resistance of candidate materials and amount of corrosion products.

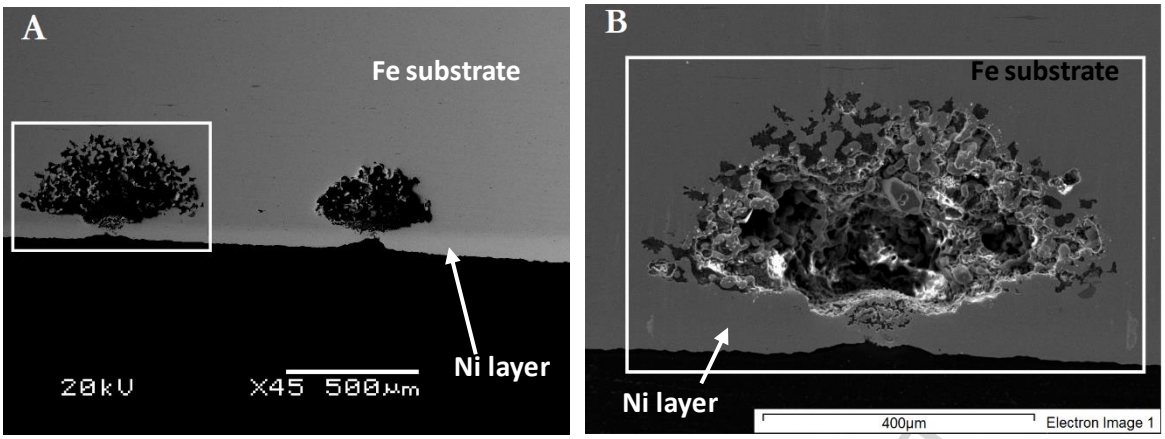

Fig. 1: Nickel-coated steel specimen after 350-hours exposure to LiF-NaF at 680 °C, corroded area EPMA image: the black area corresponds to epoxy resin, the white frames enclose the analyzed area; A) light rim on the edge of specimen – Ni coating; two perforated loci are shown; B) detail of analyzed porous cavern below the corrosion pit.

3.2. Surface analysis

Part of the sponge-like corroded area shown in Fig. 1 was subjected to quantitative elemental mapping to demonstrate penetration of MFS into the exposed specimen and to show relative depletion or enrichment of constituents in the structural material. As EPMA does not allow measuring soft radiation of light elements (in our case of Li) and fluorine ionization in the ICP source is very weak, both EPMA and LA-ICP-MS were used for obtaining 2-D elemental distributions (Fig. 2). All maps are quantified and the scale is from 0-100 $\%_{w/w}$.

The elemental maps on right hand side of Fig. 2 show the Ni coating on the steel substrate. The corrosion penetrates up to 500 µm under the Ni coating and outstanding depletion of Fe (up to 5 $\%_{w/w}$) and enrichment in Li, F and Na content. Moreover, the wide boundaries can be clearly seen between the Ni-coating and the Fe-substrate. In the outermost part of Ni-coating depletion of Ni and enrichment of Li and Na are evident.

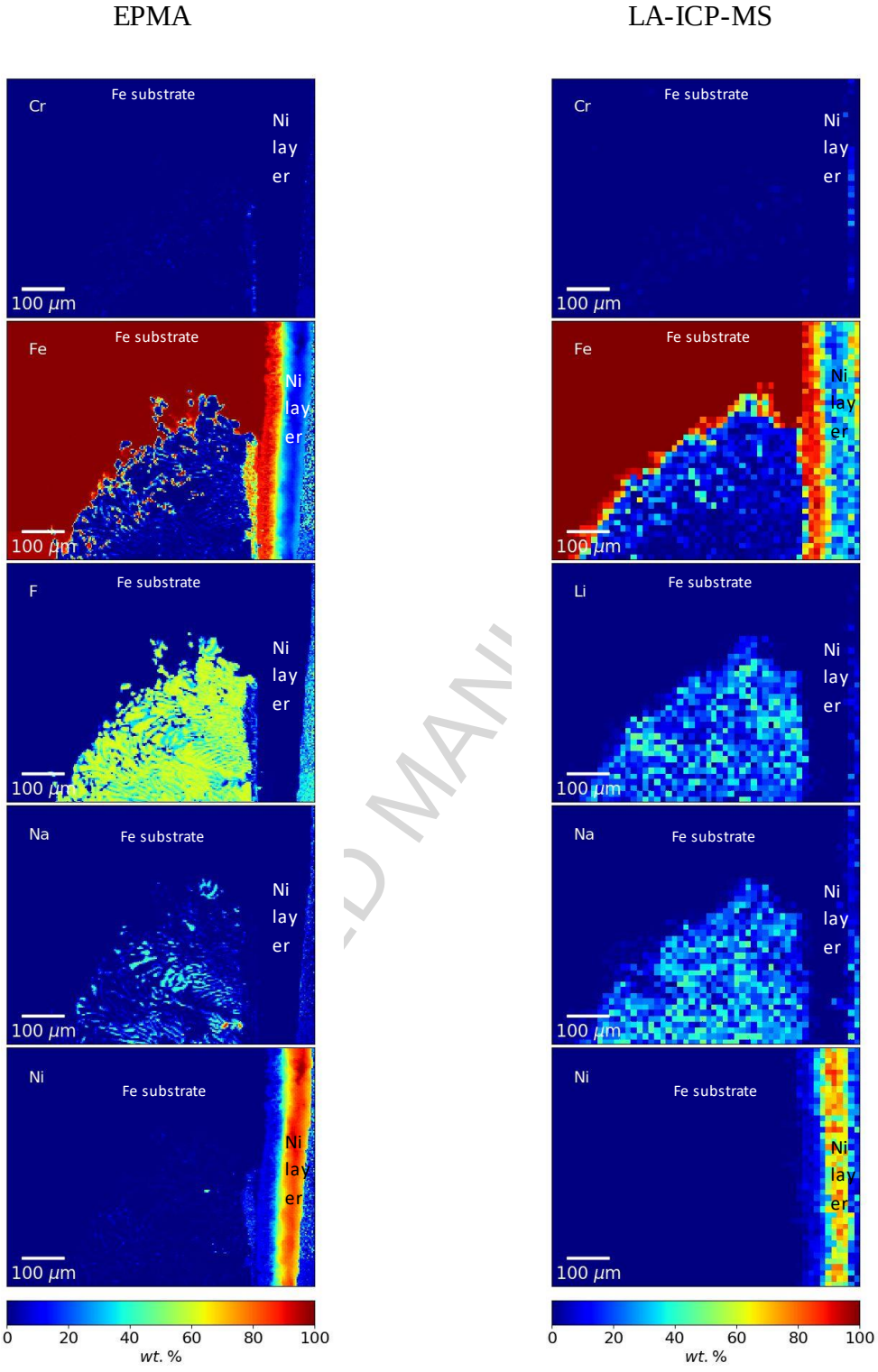

Fig. 2: Elemental maps of Cr, Fe, Li, Na and Ni obtained by LA-ICP-MS and EPM analysis of nickel-coated steel specimen after 350-hours exposure to LiF-NaF at 680 °C.

4. Conclusion

Three candidate structural materials for the nuclear industry were tested for their corrosion resistance to MFS exposure, with the most appropriate material being selected based on corrosion products content in the solidified exposed melt. The analyses show that the best candidate material is nickel, whereas the nickel alloy A071EV releases the largest amount of metals into the melt and is thus most susceptible to corrosion. A disproportionately higher amount of Fe in MSF after exposure of the Ni-coated steel specimen indicates, together with EPMA and LA-ICP-MS mapping, the coating failure followed by massive corrosion of the steel substrate to a depth of 600 μm.

Acknowledgement

This work was supported by the project CEITEC2020 (LQ1601) made by the Ministry of Education, Youth and Sports of the Czech Republic.

[1] T. Abram, S. Ion, Generation-IV nuclear power: A review of the state of the science, Energy Policy, 36 (2008) 4323-4330.
[2] J. Uhlir, Chemistry and technology of Molten Salt Reactors - history and perspectives, Journal of Nuclear Materials, 360 (2007) 6-11.
[3] R.W. Moir, Recommendations for a restart of molten salt reactor development, Energy Conversion and Management, 49 (2008) 1849-1858.
[4] C. Le Brun, Molten salts and nuclear energy production, Journal of Nuclear Materials, 360 (2007) 1-5.
[5] G. Zheng, Corrosion Behavior of Alloys in Molten Fluoride Salts, in, University of Wisconsin, 2015.
[6] J.H. Shaffer, Preparation and handling of salt mixtures for the molten salt reactor experiment, in, Oak Ridge National Laboratory; ORNL-4616, 1971, pp. 1-45.
[7] J. De Van, Effect of alloying additions on corrosion behavior of nickel-molybdenum alloys in fused fluoride mixtures, in, Oak Ridge National Laboratory; ORNL-TM-2021, 1969, pp. 1-51.
[8] L.C. Olson, J.W. Ambrosek, K. Sridharan, M.H. Anderson, T.R. Allen, Materials corrosion in molten LiF-NaF-KF salt, Journal of Fluorine Chemistry, 130 (2009) 67-73.
[9] M.W. Rosenthal, P.N. Haubenreich, R.B. Briggs, The development status of molten-salt breeder reactors, in, Oak Ridge National Laboratory; ORNL-4812, 1972.
[10] H. Trinkaus, ENERGETICS AND FORMATION KINETICS OF HELIUM BUBBLES IN METALS, Radiation Effects and Defects in Solids, 78 (1983) 189-211.
[11] L. Olson, K. Sridharan, M. Anderson, T. Allen, Nickel-plating for active metal dissolution resistance in molten fluoride salts, Journal of Nuclear Materials, 411 (2011) 51-59.
[12] V. Ignatiev, A. Surenkov, Alloys compatibility in molten salt fluorides: Kurchatov Institute related experience, Journal of Nuclear Materials, 441 (2013) 592-603.
[13] M. Liu, J.Y. Zheng, Y.L. Lu, Z.J. Li, Y. Zou, X.H. Yu, X.T. Zhou, Investigation on corrosion behavior of Ni-based alloys in molten fluoride salt using synchrotron radiation techniques, Journal of Nuclear Materials, 440 (2013) 124-128.
[14] A.K. Misra, FLUORIDE SALTS AS PHASE-CHANGE MATERIALS FOR THERMAL-ENERGY STORAGE IN THE TEMPERATURE-RANGE 1000-1400-K - THERMAL-ANALYSIS AND HEAT OF FUSION MEASUREMENTS, Journal of the Electrochemical Society, 135 (1988) 850-854.

[15] T.K. Abdullaha, C. Petitjean, P.J. Panteix, S. Mathieu, C. Rapin, M. Vilasi, Z. Hussain, A.A. Rahim, Electrochemical characterization of chromia- and alumina-forming nickel-based superalloys in molten silicates, Applied Surface Science, 360 (2016) 510-518.
[16] S. Fabre, C. Cabet, L. Cassayre, P. Chamelot, S. Delepech, J. Finne, L. Massot, D. Noel, Use of electrochemical techniques to study the corrosion of metals in model fluoride melts, Journal of Nuclear Materials, 441 (2013) 583-591.
[17] X.X. Ye, H. Ai, Z. Guo, H.F. Huang, L. Jiang, J.Q. Wang, Z.J. Li, X.T. Zhou, The high-temperature corrosion of Hastelloy N alloy (UNS N10003) in molten fluoride salts analysed by STXM, XAS, XRD, SEM, EPMA, TEM/EDS, Corrosion Science, 106 (2016) 249-259.
[18] D. Walaszek, M. Senn, M. Faller, L. Philippe, B. Wagner, E. Bulska, A. Ulrich, Metallurgical and chemical characterization of copper alloy reference materials within laser ablation inductively coupled plasma mass spectrometry: Method development for minimally-invasive analysis of ancient bronze objects, Spectrochimica Acta Part B-Atomic Spectroscopy, 79-80 (2013) 17-30.
[19] T. Vaculovic, T. Warchilova, T. Simo, O. Matal, V. Otruba, P. Mikuska, V. Kanicky, Elemental mapping of structural materials for a nuclear reactor by means of LA-ICP-MS, Journal of Analytical Atomic Spectrometry, 27 (2012) 1321-1326.
[20] R. Cerrato, A. Casal, M.P. Mateo, G. Nicolas, Dealloying evidence on corroded brass by laser-induced breakdown spectroscopy mapping and depth profiling measurements, Spectrochimica Acta Part B-Atomic Spectroscopy, 130 (2017) 1-6.
[21] M.A. Gomez-Moron, P. Ortiz, R. Ortiz, J.M. Martin, M.P. Mateo, G. Nicolas, Laser-induced breakdown spectroscopy study of silversmith pieces: the case of a Spanish canopy of the nineteenth century, Applied Physics a-Materials Science & Processing, 122 (2016).
[22] O. Matal, T. Simo, L. Nesvadba, V. Dvorak, V. Kanicky, P. Sulovsky, J. Machat, Interaction of pipeline materials with molten fluoride salts, Zeitschrift Fur Naturforschung Section a-a Journal of Physical Sciences, 62 (2007) 769-774.
[23] T. Vaculovic, P. Sulovsky, J. Machat, V. Otruba, O. Matal, T. Simo, C. Latkoczy, D. Gunther, V. Kanicky, The EPMA, LA-ICP-MS and ICP-OES study of corrosion of structural materials for a nuclear reactor cooling circuit by molten fluoride salt treatment, Journal of Analytical Atomic Spectrometry, 24 (2009) 649-654.
[24] C. Merlet, AN ACCURATE COMPUTER CORRECTION PROGRAM FOR QUANTITATIVE ELECTRON-PROBE MICROANALYSIS, Mikrochimica Acta, 114 (1994) 363-376.
[25] J.W. Koger, Evaluation of Hastelloy N alloys after nine years exposure to both a molten fluoride salt and air at temperatures from 700 to 560 °C., in, Oak Ridge National Laboratory; ORNL-TM-4189, 1972.
[26] G.Q. Zheng, B. Kelleher, G.P. Cao, M. Anderson, T. Allen, K. Sridharan, Corrosion of 316 stainless steel in high temperature molten Li2BeF4 (FLiBe) salt, Journal of Nuclear Materials, 461 (2015) 143-150.

Graphical abstract

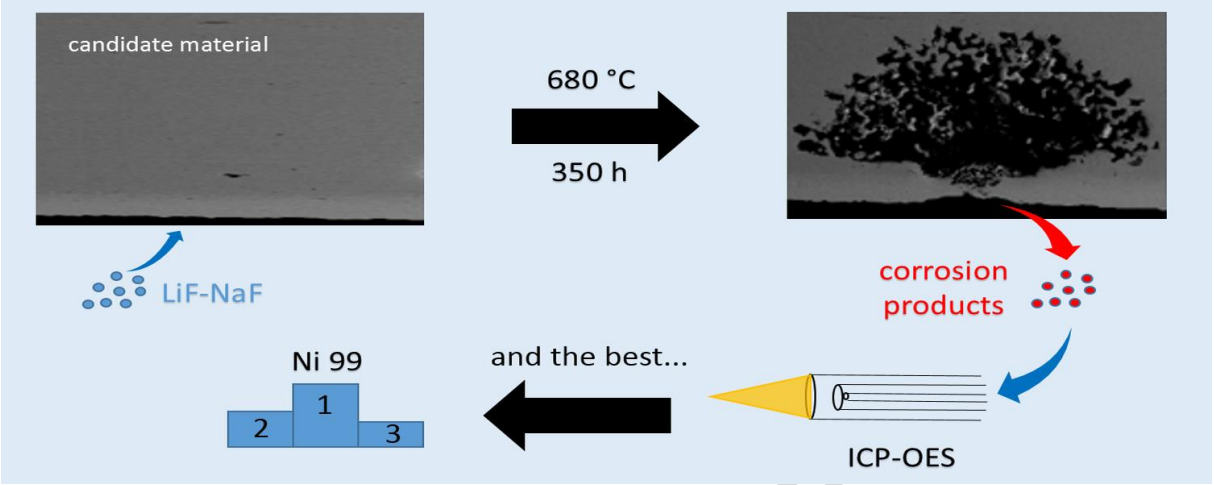

Highlights:

Corrosion of Ni-based materials induced by molten fluoride salt treatment

Analysis of corrosion products

Imaging of corrosion changes by LA-ICP-MS and EPMA